A compliantly-coupled dielectric elastomer actuator using magnetic repulsion

C. Cao, [1, 2], X. Gao, [1, 3, a)], A.T. Conn[1, 3]

1 SoftLab, Bristol Robotics Laboratory, Bristol BS16 1QY, UK

2 Department of Aerospace Engineering, University of Bristol, Bristol BS8 1TR, UK

3 Department of Mechanical Engineering, University of Bristol, Bristol BS8 1TR, UK

Abstract Dielectric elastomer actuators (DEAs) have attracted growing research interest over the past two decades for their large actuation strain, inherent compliance and low cost. The conical DEA configuration is particularly attractive thanks to its simple structure and high force/stroke actuation. A double cone DEA design with two antagonistic membranes allows active bidirectional actuation. However, in existing double cone DEA designs, the two membranes are rigidly coupled which restricts their relative actuation response under periodic electrical input to 180˚ out-of-phase operation. This work presents a magnetically-coupled DEA (MCDEA) with compliant coupling by a magnetic repulsion. The compliant coupling allows two separate inputs with a fully adjustable phase difference. The current prototype demonstrates a peak normalized stroke of 14% (relative to nominal DEA height) at a phase shift of 180° and a normalized linear expansion between the two membranes of up to 8.3% (relative to nominal DEA height) at a phase shift of 0° at 0.5 Hz. This results in several emerging actuation behaviors, which could potentially be suitable for controllable shape changing actuations, active vibration damping and bioinspired locomotion.

Dielectric elastomer actuators (DEAs) are an emerging type of actuation technology that demonstrate advantages over conventional actuators in terms of large actuation strain, inherent compliance and low cost [1]. Many DEA-based applications have been documented, such as grippers [2-5], generators [6-8] and robotic locomotion [9]. The basic structure of a DEA consists of a dielectric elastomer membrane sandwiched by compliant electrodes; when subjected to an electric field, the generated Maxwell pressure causes the membrane to expand in area and compress in thickness. Based on this transduction mechanism, various DEA configurations have been developed [10] and, among them, the conical DEA configuration (known as a *cone DEA*) has been widely adopted in applications such as soft pumps [11], high-speed positioning

[a)] Xing Gao xing.gao@bristol.ac.uk

systems [12] and walking robots [9]. A cone DEA includes an elastomer membrane bonded to a rigid circular frame. A rigid disk is bonded to the centre of the membrane and a biasing element generates a protrusion force acting on the central disk that deforms the membrane out-of-plane into a conical geometry. Such a structure has advantages of low cost, ease of fabrication and high force/stroke actuation [13-15].

A core part of a cone DEA is the biasing element, which may be a linear compression spring [16], a deadweight [17,18], a bistable mechanism [17,18], a magnetic force [14,15,19], or an antagonistic DEA membrane [20-24]. A cone DEA with a biasing weight has been shown to have a greater stroke than that with a linear compression spring [19,25]. However, the weight significantly increases the mass of the actuator and the gravitational force restricts its orientation and application. The use of a magnetic attraction force can amplify the stroke of the cone DEA and it has been shown that permanent magnet biasing mechanisms can outperform equivalent spring-biased designs[19]. The biasing force from coupling an antagonistic DEA membrane pair creates a double cone design (known as a *double cone DEA*). The antagonistic coupling in double cone DEAs is conventionally achieved by a rigid attachment between the two DEA membranes [21,22,26], which means they must be actuated 180˚ out-of-phase to generate a maximal stroke. While rigidly-coupled double cone DEAs can generate antagonistic actuation, as demonstrated in applications such as crawling [9] and flapping wing robotics locomotion [24], if both membranes are activated simultaneously in-phase, no output stroke is generated, so the configuration can be considered to have a single modality.

Here, we present a magnetically-coupled DEA (MCDEA) where the two membranes are compliantly-coupled using the repulsion of two permanent magnets, as shown in FIG. 1. The reaction force of the DEA membrane being deformed out-of-plane, F_{DEA}, and the magnetic repulsion, F_{Mag}, is balanced in its passive state (FIG. 1(b)). When a voltage applied across the DEA membrane, the reaction force exerted by the membrane reduces (as shown supplementary FIG. S1(a-c)). The force imbalance between the F_{Mag} and the F_{DEA} causes the membrane to deform out-of-plane further until another force balance is achieved (FIG. 1(c-d)).

By using this compliant coupling, this MCDEA has the capacity for different modalities when the electrical inputs to each membrane are given an adjustable phase difference between them from 0˚ to 360˚, which can result in several emerging actuation behaviours. For example, when the actuation voltages on the two membranes are in-phase, the double cone DEA expands in both directions (FIG. 2(a-c)). Alternatively, when the actuation voltages are 180˚ out-of-

phase, the DEA cones expand on one side and shorten on the other (FIG. 2d-f). The coupling mechanism using magnetic field instead of a solid structure also allows applications where the actuator end-effector can be on either the outside or inside of the membranes. In this work, the quasi-static and dynamic performance of the presented MCDEA is characterized and the effects of pre-stretch ratio on the MCDEA's performance is investigated. Finally, we demonstrate a modulated phase shift between the two inputs from 0˚ to 330˚ and analyse the effect on the performance of the DEA.

As illustrated in FIG. 1(b-d), the proposed MCDEA is an electromechanical-magnetic coupled system. From an energy point of view, this system consists of the strain potential energy of the two membranes U_{strain}, magnetic potential energy of the two magnets U_{mag} and the electric potential energy U_{ele} of the DEA. The strain potential energy was estimated by [16]

$$\begin{aligned} \lambda_1 &= \sqrt{\frac{(b-a)^2+\left(\frac{s_0}{2}+d\right)^2}{b-a}}\,\lambda_{pre} \\ \lambda_2 &= \lambda_{pre} \\ U_{strain} &= \sum \frac{2\pi t_0}{\lambda_1 \lambda_2}\int_a^b W\,R\,dR \end{aligned}, \tag{1}$$

where the summation symbol represents the summation of two membranes; λ_1 and λ_2 are the in-plane principle stretches; a is the radius of magnet and b is the inner radius of the outer frame; s_0 is the initial distance between two magnets; d is the displacement of output 1 or 2 (FIG. 1(b and d)); λ_{pre} describes the pre-stretch.

The free energy density of ideal dielectric elastomer W can be presented by the Gent model [27],

$$W(\lambda_1,\lambda_2) = -\frac{\mu J_{\lim}}{2}\log\left(1-\frac{\lambda_1^2+\lambda_2^2+\lambda_1^{-2}\lambda_2^{-2}-3}{J_{\lim}}\right), \tag{2}$$

where μ is the shear modulus of the elastomer; $J_{\lim}$ is the constant related to the limiting stretch. The electric potential energy is calculated by

$$U_{ele} = \frac{1}{2}\sum CV^2\ , \tag{3}$$

where *C* is the capacitance, *V* is the applied voltage. The magnetic potential energy U_{mag} is caused by the repulsive magnetic pair, and can be defined as [14],

$$U_{mag} = \frac{\mu_0 m_1 m_2}{2\pi\left(s_0 + d_1 + d_2\right)^3}, \quad (4)$$

where μ_0 is the permeability of vacuum; m_1 and m_2 are the magnetic moments of the magnets on the two membranes; d_1 and d_2 are displacements of the two outputs (FIG. 1(d)), respectively.

FIG. 2 shows an example to estimate fluctuation of the strain potential energy δU_{strain}, the electric potential energy δU_{ele}, and the magnetic potential energy δU_{mag} of the whole system with a phase shift of 0° (FIG. 2(a-c)) and 180° (FIG. 2(d-f)) during an actuation cycle with a sinusoidal voltage wave form (values were estimated using equations 1-4 with experimentally measured displacements and voltages). As can be seen, as the actuation voltage is applied, the potential electrical energy increases while the magnetic potential energy is converted into elastic potential energy of the membranes. It can be noted that when phase shift is 0°, only one peak can be observed in the energy conversion plot in one cycle (FIG. 2(c)), which is due to synchronized two inputs (FIG. 2(a-b)). However, as the two inputs become 180° out-of-phase (FIG. 2(d-e)), two separate peaks can be observed in one cycle and the change in elastic potential energy and magnetic potential energy becomes smaller than in the case of 0°, as illustrated in FIG. 2(f). It can also be seen that there is a small delay between the peak strain potential energy after the peak electrical potential energy, which is due to the viscoelasticity of the DEA membrane. In addition, in-phase and 180° out-of-phase force balance can be found in supplementary FIG. S2 and S3 respectively, suggesting the magnetic repulsion serves to adapt voltage induced membrane tension until a new force equilibrium state.

The fabrication process of the MCDEA is described as follows. Firstly, an off-the-shelf silicone elastomer (Elastosil, thickness = 100 μm, Wacker Chemie AG) was pre-stretched biaxially, then bonded to an acrylic frame with an inner diameter of 40 mm by silicone transfer tape (ARclear 93495, Adhesives Research). Two 15 mm diameter × 0.5 mm thick disc magnets (0.28 × 2 kg pull force, First4Magnets, repulsion was measured shown in supplementary FIG. S1(d)) were attached to the centre of the membrane using the same method. The selected ratio of magnet to DEA membrane diameters, equal to 0.375, was found to generate reliable and stable operation. Conductive carbon grease (MG Chemicals) was hand-brushed on each side of the membrane as the compliant electrodes. Two DEA membranes were fabricated

separately, and their acrylic frames were connected using bolts and fasteners. To compliantly-couple the two DEA membranes, the magnets were positioned to ensure the same poles are facing each other such that the membranes are deformed out-of-plane by repulsion. Three prototypes of DEAs with different pre-stretch ratios were fabricated: λ_p = 1.2 × 1.2, λ_p = 1.3 × 1.3 and λ_p = 1.4 × 1.4.

A force-displacement test was performed to characterise the passive stiffness of the DEA. The DEA frame was fixed to the testing rig (detailed experimental setup can be found in supplementary FIG. S3). A linear rail (X-LSQ150B-E01, Zaber Technologies Inc.) deformed the end-effector (magnet) on one side at a constant velocity of 0.01 mm/s while the passive reaction force was measured by a load cell (NO.1004, Tedea). The force-stroke response when the DEA is actuated was investigated as follows. A nominal electric field E_n = 70 V/μm was applied by a high voltage amplifier (Ultravolt, 5HV23-BP1) to one DEA membrane which generated a force and stroke on the end-effector. The load cell was used to measure the force generated at a position from zero to the maximum stroke while a laser displacement sensor (LK-G152 and LKGD500, Keyence) measured the corresponding position. All data was collected by a DAQ device (National Instruments, BNC-2111) and experiments were controlled by MATLAB (Mathworks). The measured passive force-displacement and active force-stroke relationships are plotted in FIG. 3(a)-(b), respectively. It can be seen from FIG. 3(a) that the passive force-displacement relationship is approximately linear for all three prototypes and, as the pre-stretch ratio increases, the DEA becomes effectively stiffer. The small hysteresis loop suggests a limited damping behaviour in the system. In FIG. 3(b), the active force-stroke relationship is also approximately linear, as has been demonstrated in our previous double cone DEA design [26]. It can be noted that under the same nominal electric field, the prototype with the lowest pre-stretch ratio has the best force-stroke output, which suggests the maximum work output of this DEA prototype is also the highest.

Silicone-based DEAs have reduced viscoelastic damping, which enables an increased actuation stroke at resonance [24]. Here we characterize the dynamic response of the proposed DEA using an experimental approach. A sinusoidal driving voltage of $V(t) = \frac{V_{peak}}{2} + \frac{V_{peak}}{2} \sin 2\pi\Omega t$ with the frequency, Ω, stepped up from 1 to 150 Hz with increments of 0.1 Hz was applied to one membrane in the double cone DEA and at each frequency 10 cycles were repeated to ensure the DEA reached a steady-state response. A nominal electric field of E_n = 60 V/μm was adopted in this experiment which resulted in a peak voltage, $V_{peak} = E_n T_0 / \lambda_p^2$

(where T_0 is the initial thickness of the DEA membrane, assuming an incompressible elastomer with principal stretches $\lambda_1\lambda_2\lambda_3 = 1$). FIG. 3(c) plots the amplitude against excitation frequency for the three prototypes. Three amplitude peaks can be observed for each prototype and this type of behaviour is expected in dynamic systems with more than one elastic element in series [28]. As the pre-stretch ratio increases, the peak reduces significantly while the corresponding resonant frequency increases. For the prototype with λ_p = 1.2 × 1.2, the three peaks have the amplitudes of 1.77 mm, 4.06 mm and 1.27 mm at 23.5 Hz, 46.1 Hz and 87.6 Hz respectively, where the second peak is believed to be the resonant frequency of the DEA.

One of the biggest advantages of a double cone DEA is the antagonist actuation [25]. Here we analyse the effect of phase shift of the two inputs on the performance of the proposed DEA. Tests were performed with the phase shift $\Delta\phi$ from 0˚ (synchronized) to 330˚ with an increment of 30˚ (FIG. 5 (Multimedia view). Actuation voltages and the corresponding displacements of the two membranes can be found in supplementary FIG. S4-6. The actuation waves for the two membranes are written as follows: $V_1(t) = \frac{V_{peak}}{2} + \frac{V_{peak}}{2}\sin(2\pi\Omega t)$, $V_2(t) = \frac{V_{peak}}{2} + \frac{V_{peak}}{2}\sin\left(2\pi\Omega t + \frac{\Delta\emptyset}{2\pi}\right)$, where Ω = 0.5 Hz. The prototype with λ_p = 1.2 × 1.2 was used in this experiment due to the best performance among all three prototypes. Two laser displacement sensors were utilized to measure the displacements of the two outputs independently. Due to the compliant-coupling between the two DEA membranes, during actuation the distance between the two magnets can change and the variation of distance between the two magnets Δs demonstrates the coupling between the two outputs.

FIG. 4 shows the two outputs and the variation of Δs with phase shift from 0˚ to 330˚ at 0.5 Hz. The smallest and largest stroke for both outputs occurred at $\Delta\phi$ = 0° and 180° respectively. Also, it can be noted that stroke 2 is larger than stroke 1 in a range from $\Delta\phi$ = 0° to 180° and, as there is a further increase in $\Delta\phi$, stroke 1 becomes larger (FIG. 4(a)). Δs is found to have the highest and lowest value at $\Delta\phi$ = 0° and 180° respectively (FIG. 4(b)) since the two membranes are synchronized at $\Delta\phi$ = 0° (FIG. 4(c) and (e)) and alternate at $\Delta\phi$ = 180° (FIG. 4(d) and (f)).

In summary, we have presented MCDEA with compliant coupling by magnetic repulsion. In contrast to rigidly-coupled double cone DEAs, the compliant magnetic coupling enables multi-modal operation where a single reciprocating output or two separate outputs are achievable from the same actuator. Quasi-static tests showed that both the passive force-

displacement response and active force-stroke output demonstrated an approximately linear relationship. Resonant excitation was demonstrated with a significant increase in the actuation stroke in such dynamic tests. By comparing both the quasi-static and dynamic performances of the three prototypes with different pre-stretch ratios under the same nominal electric field, it was found that a higher pre-stretch ratio can result in a 'stiffer' DEA with a higher resonant frequency but a lower maximum work output and a lower resonant amplitude. Exploiting the compliantly-coupled mechanism, we demonstrated an adjustable phase shift between the two outputs which could not be achieved using previous rigidly-coupled double cone DEA designs. This phase control scheme of two outputs from a single DEA offers an alternative approach towards potential applications such as active vibration absorption and gait changes in biomimetic locomotion, while the active expansion generated from in-phase activation of the two membranes can potentially be exploited for active shape changes in applications such as DEA-driven suction cups [29].

C. Cao appreciates the support from the EPSRC Centre for Doctoral Training in Future Autonomous and Robotic Systems (FARSCOPE) at the Bristol Robotics Laboratory. A. Conn and X. Gao acknowledge support from EPSRC grant EP/P025846/1.

1 R. Pelrine, R. Kornbluh, Q. Pei, and J. Joseph, Science **287**, 836 (2000).

2 G.K. Lau, K.R. Heng, A.S. Ahmed, and M. Shrestha, Appl. Phys. Lett. **110**, 182906 (2017).

3 J. Shintake, S. Rosset, B. Schubert, D. Floreano, and H. Shea, Adv. Mater. **28**, 231 (2016).

4 G. Kofod, W. Wirges, M. Paajanen, and S. Bauer, Appl. Phys. Lett. **90**, 081916 (2007).

5 X. Gao, C. Cao, J. Guo, and A.T. Conn, Elastic Electroadhesion with Rapid Release by Integrated Resonant Vibration, Adv. Mater. Technol. (2018) (in press).

6 S.J.A. Koh, X. Zhao, and Z. Suo, Appl. Phys. Lett. **94**, 262902 (2009).

7 T. McKay, B. O'Brien, E. Calius, and I. Anderson, Appl. Phys. Lett. **97**, 062911 (2010).

8 T.G. McKay, B.M. O'Brien, E.P. Calius, and I.A. Anderson, Appl. Phys. Lett. **98**, 142903 (2011).

9 C.T. Nguyen, H. Phung, T.D. Nguyen, H. Jung, and H.R. Choi, Sens. Actuators A Phys. **267**, 505 (2017).

10 I.A. Anderson, T.A. Gisby, T.G. McKay, B.M. O'Brien, and E.P. Calius, J. Appl. Phys., **112**, 041101 (2012)

[11] F.A.M. Ghazali, C.K. Mah, A. AbuZaiter, P.S. Chee, and M.S.M. Ali, Sens. Actuators A Phys. **263**, 276 (2017).

[12] S. Hau, G. Rizzello, M. Hodgins, A. York, and S. Seelecke, IEEE-ASME T. Mech. **22**, 1259 (2017).

[13] S. Hau, D. Bruch, G. Rizzello, P. Motzki, and S. Seelecke, Smart Mater. Struct. **27**, 074003 (2018).

[14] X.Q. Li, W.B. Li, W.M. Zhang, H.X. Zou, Z.K. Peng, and G. Meng, Smart Mater. Struct. **26**, 105007 (2017).

[15] T. Yang, Y. Xiao, Z. Zhang, Y. Liang, G. Li, M. Zhang, S. Li, T.W. Wong, Y. Wang, and T. Li, Sci. Rep. **8**, 14518 (2018).

[16] M. Hodgins, G. Rizzello, D. Naso, A. York, and S. Seelecke, Smart Mater. Struct. **23**, 104006 (2014).

[17] M. Hodgins, A. York, and S. Seelecke, Smart Mater. Struct. **22**, 094016 (2013).

[18] C. Zhang, W. Sun, H. Chen, L. Liu, B. Li, and D. Li, J. Appl. Phys. **119**, 094108 (2016).

[19] P. Loew, G. Rizzello, and S. Seelecke, Mechatronics **56**, 48 (2018)

[20] M. Follador, M. Cianchetti, and B. Mazzolai, Meccanica **50** (11), 2741 (2015).

[21] H.R. Choi, K.M. Jung, J.W. Kwak, S.W. Lee, H.M. Kim, J.W. Jeon, and J.D. Nam, in *Robotics and Automation 2003: Proceedings of 2003 IEEE International Conference on Robotics and Automation (ICRA'03)*, Taipei, Taiwan, September 14-19, pp. 1857-1862 .

[22] A.T. Conn and J. Rossiter, Smart Mater. Struct. **21**, 035012 (2012).

[23] F. Branz and A. Francesconi, Smart Mater. Struct. **25**, 095040 (2016).

[24] C. Cao, S. Burgess, and A.T. Conn, in *2018 IEEE International Conference on Soft Robotics (RoboSoft)*, Livorno, Italy, April 24 – 28 2018, pp. 327-332.

[25] M. Hodgins, G. Rizzello, A. York, D. Naso, and S. Seelecke, Smart Mater. Struct. 24, 094002 (2015).

[26] A.T. Conn and J. Rossiter, in *Electroactive Polymer Actuators and Devices (EAPAD) 2011*, San Diego, US, March 7-10 2011.

[27] A.N. Gent, Rubber Chem. Technol. **69**, 59 (1996).

[28] A. Ruina and R. Pratap, Introduction to Statics and Dynamics (Oxford University Press, 2010), p. 412–530.

[29] M. Follador, F. Tramacere and B. Mazzolai, Bioinspir. Biomim. **9**, 046002 (2014).

Figures

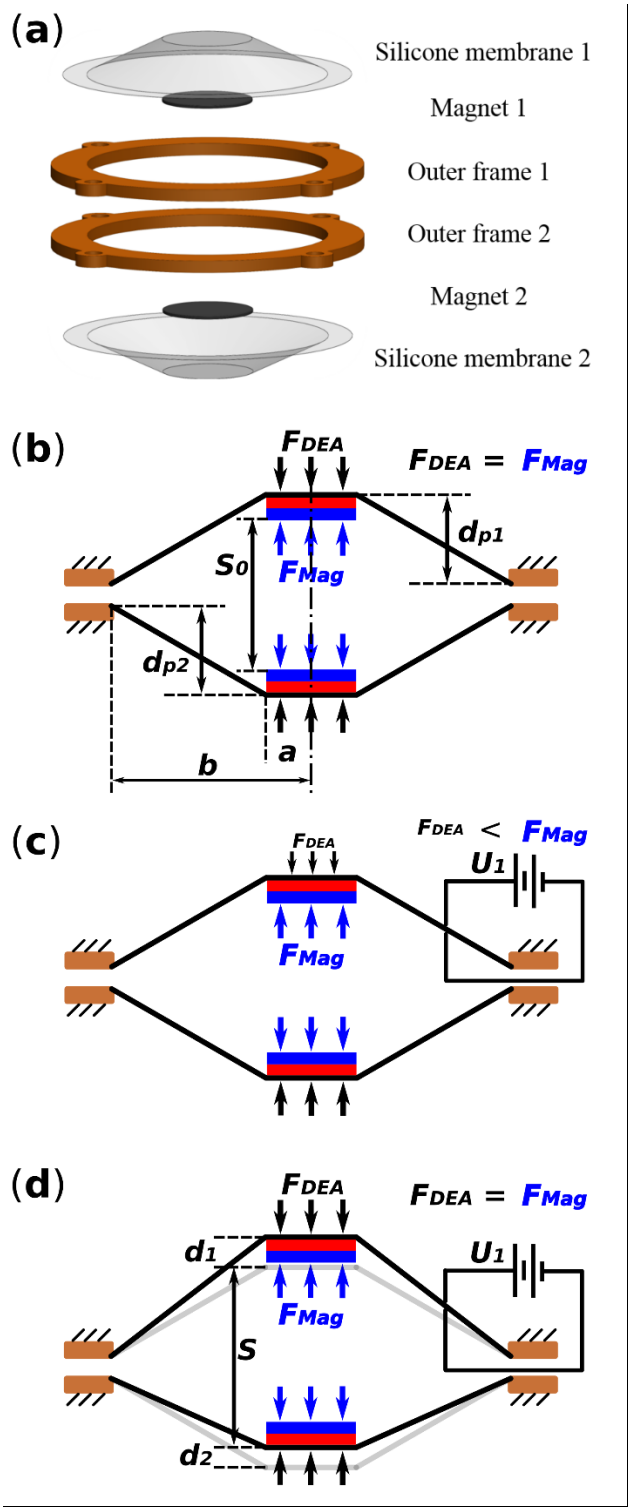

FIG. 1. (a) Structure of the MCDEA (for clear demonstration, electrodes are in absence). (b) Two membranes with a central thin magnet are face to face to form a double conical geometry under magnetic repulsive force. When a voltage applied across upper membrane, (c) the force imbalance between the F_{Mag} and the F_{DEA} is caused due to the induced Maxwell pressure (d) and the membrane deforms out-of-plane further until another force balance is achieved.

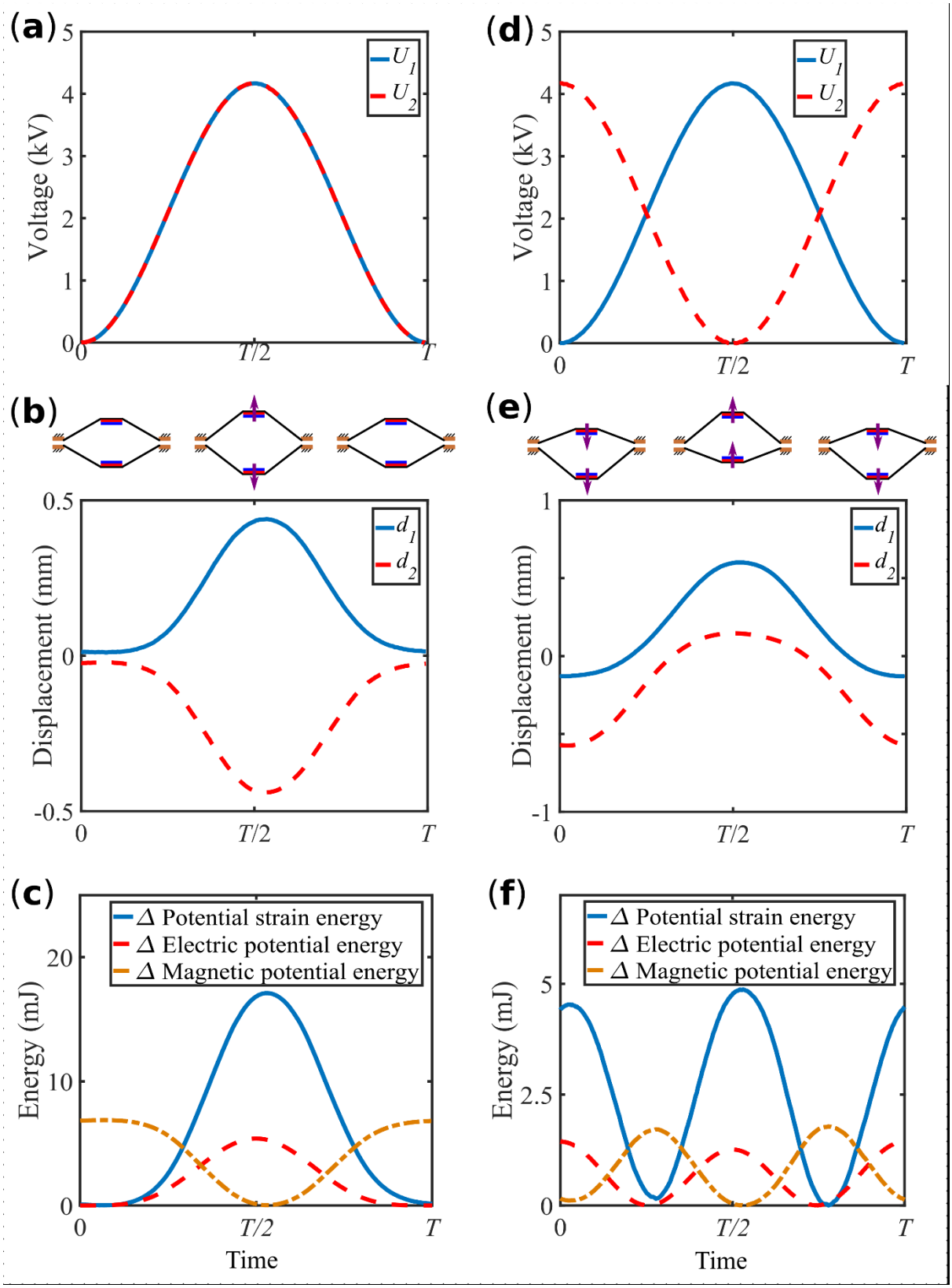

FIG. 2. An example of the applied voltages, measured displacement and energy change in the MCDEA during the actuation at phase difference 0° (a), (b) and (c), respectively and 180° (d), (e) and (f), respectively (note that all energy values were estimated based on experimental results).

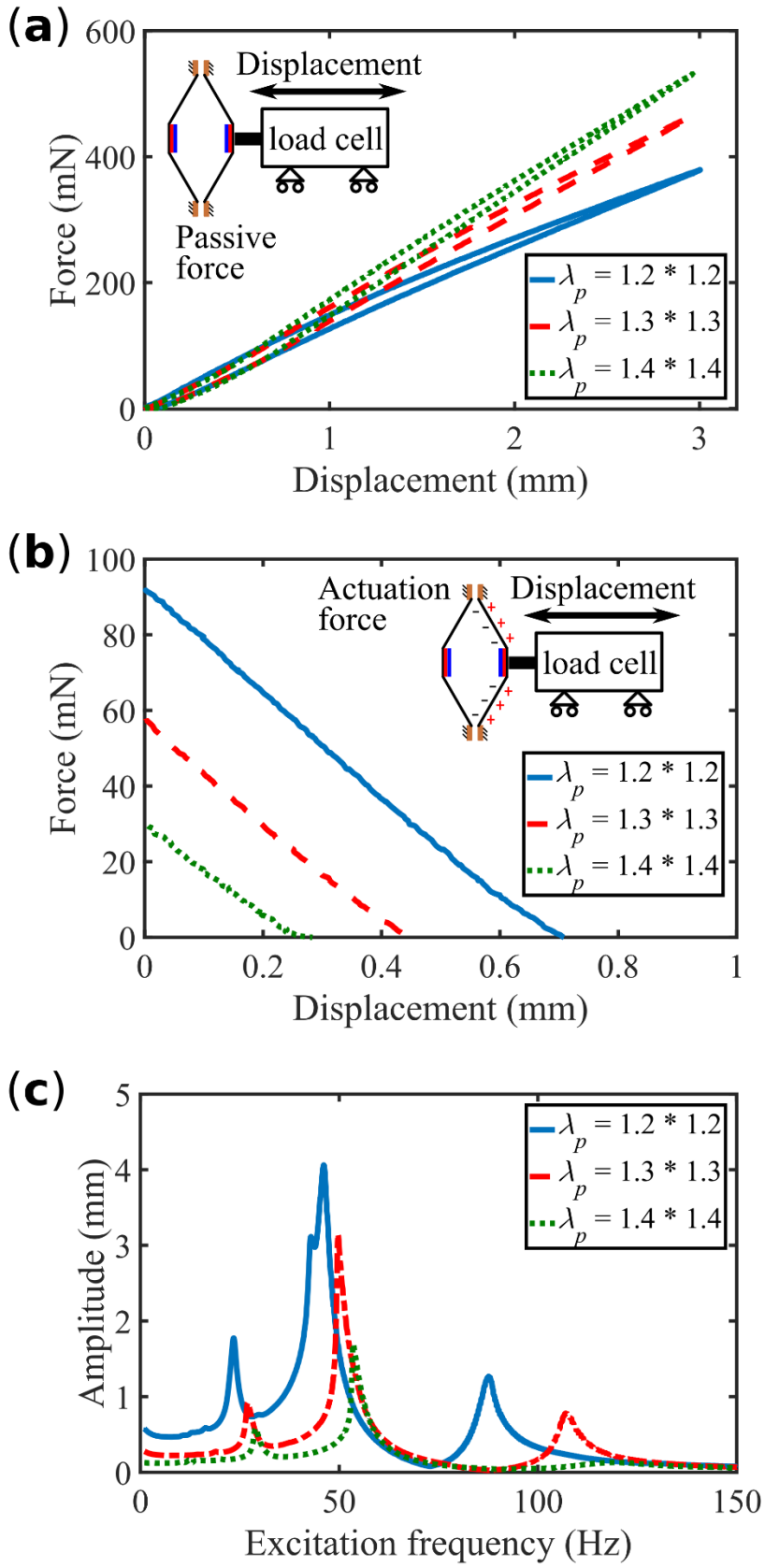

FIG. 3. Response characterization of the MCDEA – (a) passive force-displacement and (b) active force-stroke output – and (c) dynamic response of the DEA with various pre-stretch ratios of λ_p = 1.2 × 1.2, λ_p = 1.3 × 1.3 and λ_p = 1.4 × 1.4.

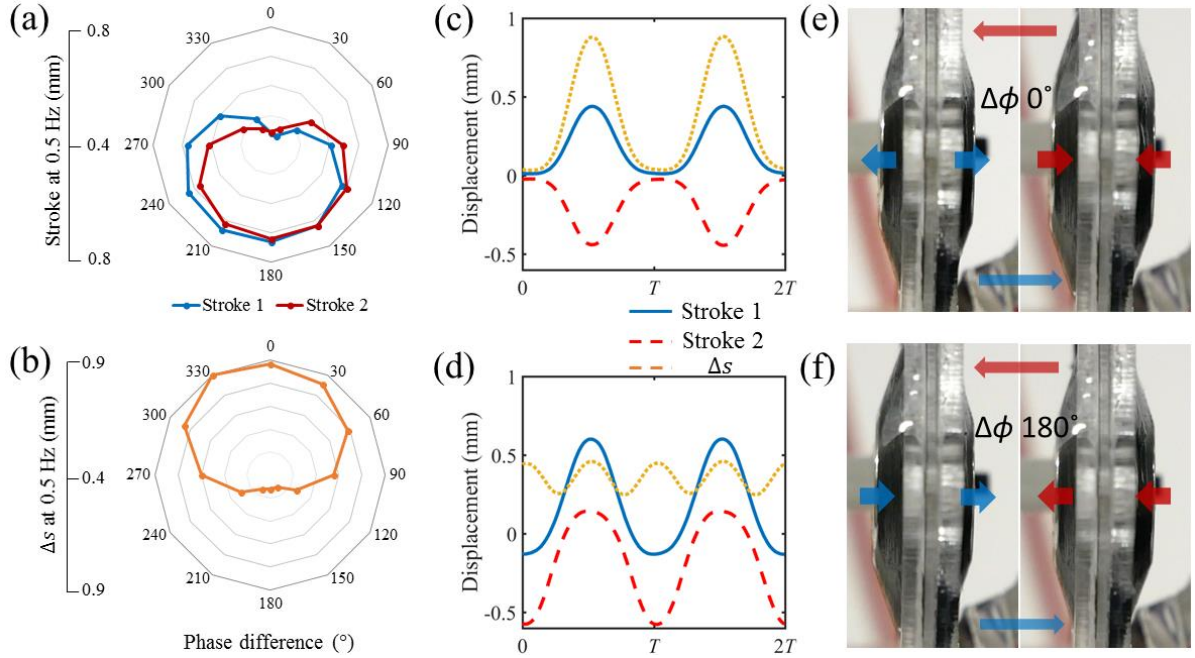

FIG. 4. Actuation performances of the MCDEA at 0.5 Hz – (a) stroke of the two membranes, (b) distance between the two magnets Δs – as a function of phase difference and time series of strokes and Δs at (c) $\Delta\phi$ 0° and (d) $\Delta\phi$ 180°; Images show the actuation performances at (e) $\Delta\phi$ 0° (the two membranes are synchronized) and (f) $\Delta\phi$ 180° (the two membranes are alternated).